

Self-Assembly of Gold Nanoparticles Induced by Poly(oxypropylene)diamines

Hsin-Yeh Huang, Wei-Fu Chen, and Ping-Lin Kuo*

Department of Chemical Engineering, National Cheng Kung University, Tainan, Taiwan 70101, Republic of China

Received: July 14, 2005; In Final Form: November 1, 2005

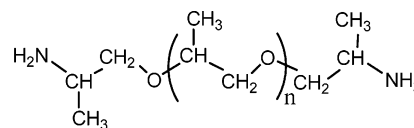
A series of poly(oxypropylene)diamines D230, D400, D2000, and D4000, having molecular weights of hydrophobic segments of 230, 400, 2000, and 4000, were used as ligands to synthesize self-organized gold nanocrystals. Ligand exchange significantly reduced the average particle size and the polydispersity of nanocrystals, and this effect was more remarkable as the molar ratio of amine groups to Au^{3+} ions ($[\text{N}]/[\text{Au}^{3+}]$ ratio) was increased. Under the same $[\text{N}]/[\text{Au}^{3+}]$ ratio of 100, D2000 generated an ordered 2D-monolayer; however, D230 and D400 colloids formed mainly a densely packed 3D structure with minor 2-D layers, and D4000 presented disordered 3D and 2D structures. The gap among the nanoparticles was found to be increased with the increasing molecular weight of the hydrophobic segment of ligands, accompanied by the decreasing wavelength of UV–vis absorption bands. This increased gap can be interpreted as the ligand thickness calculated from the equation of steric force increasing with increasing molecular weight of the hydrophobic segment. The potential energies obtained from the calculated ligand thickness according to the soft sphere model show more steep potential wells for D230 and D400 colloids than that for the D2000 colloid. This explains why the aggregation hardly occurred for the gold nanoparticles obtained under D2000, where the nanoparticles are single crystals having face center crystal structure with a lattice constant of 2.36 Å and have grain sizes close to the average particle sizes, evidenced from the results of transmission electron microscopy and X-ray diffraction spectroscopy.

Introduction

The capability of colloidal metal nanocrystals to spontaneously form organized structures has been the subject of intensive research.¹ These ordered structures reported in the literature have been obtained either by the self-organization of particles capped with alkyl chains or by assembly on modified substrates.^{2–4} In each case, the ligand played an important part in influencing the ordered packing. Several research groups have evaluated the effects of variable chain length—alkyl^{5–7} or aromatic,⁸ thiols or dithiols, alkylamines,⁹ ammonium salts,^{11–13} and alkyl silanes¹⁴—on the self-assembly of nanocrystals. For the alkanethiols, the particle size and the interparticle distances were reported to increase and then to reach a maximum as the alkyl chain length increased.¹⁵ It would be interesting to know whether any hydrophobic segment other than the alkyl chain could also induce ordered assemblies and how the chain length affects the particle sizes and gaps.

The amino group, which has been reported to interact with metal ions¹⁶ as well as with the corresponding reduced metal,^{17–21} can be expected to play a significant role in the formation of self-assemblies, as the molecular configurations and the intermolecular interactions of difunctional polyoxypropylenated diamines are totally different from those of monofunctional alkyl chains. In the present work, a series of poly(oxypropylene)diamines (D230, D400, D2000, and D4000) were used as the ligands to induce gold nanoparticles to self-assemble into well-ordered structures. The effect of the arrangement of ligand molecules with different chain lengths on the confined surfaces between two nanocrystals is most notable.

CHART 1: Structure of Poly(oxypropylene)diamines



average molecular weight: 230, 400, 2000 and 4000 g/mol

Transmission electron microscopy (TEM), selected-area electron diffraction (SAED), X-ray diffraction (XRD), and absorption spectroscopy were used to characterize the assemblies. It was found that these nanocrystals self-assemble into monolayers or multilayers after the ligand-exchange process, and the particle sizes, interparticle distances, and absorption band wavelengths are highly dependent on the chain length. Several kinds of organizational models for the poly(oxypropylene)diamine molecules are proposed in an attempt to explain the particle gap and van der Waals potential of the self-assembly of nanocrystals in the observed structures.

Experimental Section

Materials. Poly(oxypropylene)diamines, including D230, D400, D2000, and D4000, were supplied from Huntsman Corporation. Fresh aqueous solutions of hydrogen tetrachloroaurate ($\text{HAuCl}_4 \cdot 4\text{H}_2\text{O}$, SHOWA Chemicals) were prepared for every synthesis. Trisodium citrate was purchased from Aldrich. All chemicals were used as received without further purification. The water used throughout all experiments was purified through a Milli-Q system.

Synthesis of Ligand-Modified Gold Nanoparticles. The chemical structure of poly(oxypropylene)diamine was shown in Chart 1, where n represents the repeating oxypropylene group

* To whom all correspondence should be addressed. Phone: +886-6-275-7575, ext 62658. Fax: +886-6-276-2331. E-mail: plkuo@mail.ncku.edu.tw.

on the polymer backbone. The average molecular weights are 230, 400, 2000, and 4000 g/mol for D230, D400, D2000, and D4000. Ligand-modified Au nanoparticles were prepared according to the following procedures.^{22,23} Typically, 50 mL of 10^{-4} M HAuCl₄ aqueous solution was prepared, followed by adding 2×10^{-4} mol of trisodium citrate at 100°C with stirring under reflux for 30 min. Finally, a transparent deep red solution of gold colloids was obtained. The as-prepared colloidal solution thus formed was then spilt into 5 mL portions. Poly(oxypropylene)diamine, being dissolved in a 5 mL ethanol solution, was added to each portion keeping the molar ratio of HAuCl₄ to ligand molecule of 0.01. This ligand exchange process caused an immediate color change from deep red to blue except for D2000 and D4000, which change to pink instead. All the samples were purified by the precipitation method twice. Particle aggregates caused by centrifugation settled down to the bottom of the vial, leaving extra ligands and side products in the top supernatant layer. After the top supernatant layer was decanted, the bottom precipitates were re-dispersed into 5 mL of ethanol for the second purification. The colloids passivated by D230, D400, D2000, and D4000 are designated as Au-D230, Au-D400, Au-D2000, and Au-D4000, respectively, to facilitate discussion.

Characterizations. The Au colloidal solutions before and after ligand exchange were measured at room temperature by a Beckman Coulter DU-800 spectrophotometer. Transmission electron micrographs were taken with a JEOL JEM 1200-EX transmission electron microscope (TEM) operating at 80 kV. High-resolution transmission electron microscopy (HR-TEM) was performed with a Hitachi Model HF-2000 field emission transmission electron microscope at 200 kV for analyzing the lattice structures and the selected area electron diffraction (SAED) patterns. Specimens were prepared by placing a drop of the colloidal solution onto 200-mesh copper grids coated with an amorphous Formvar carbon film and allowing the solvent to evaporate. The mean diameters and size distributions of Au nanoparticles were calculated on the basis of the measurement of at least 200 particles. The standard deviations of the size distribution were calculated from the same equation that has been commonly used in the literature. X-ray diffraction (XRD) was carried out by using a Rigaku RINT2100 X-ray diffractometer with reflection geometry and Cu K α radiation (wavelength $\lambda = 0.154$ nm) operated at 40 kV and 40 mA. The data were collected within the range of the scattering angles (2θ) of 2–90°.

Results and Discussion

Morphology and Optical Properties of Amine-Stabilized Au Nanocrystals. In our investigation, we prepared amine-stabilized gold colloids using poly(oxypropylene)diamine ligands for two reasons. First, the orientations adopted by the poly(oxypropylene) (POP) structure are likely to be very different from those of the more widely used alkyl chains due to both the flexibility of the $-\text{CH}_2\text{CH}(\text{CH}_3)\text{O}-$ group and its intermolecular interactions, and second, we wanted to achieve the arrangement of POP chains, with different chain lengths, on a confined dimension between two spherical surfaces. Images of gold colloids formed simply by mixing sodium citrate and HAuCl₄ are shown in Figure 1a. The shapes of the nanocrystals, which form random agglomerations, are typically spherical or polyhedral, with average diameters of 14.2 ± 1.5 nm. The addition of ligands, e.g., D2000, to the citrate-stabilized colloid at room temperature induces drastic changes in both the morphology and the size of these nanocrystals (Figure 1b). No longer seen are the agglomerated particles; instead, well-distributed spherical nanocrystals with smaller sizes (10.5 ± 0.8 nm) are found to be arranged in a well-ordered fashion.

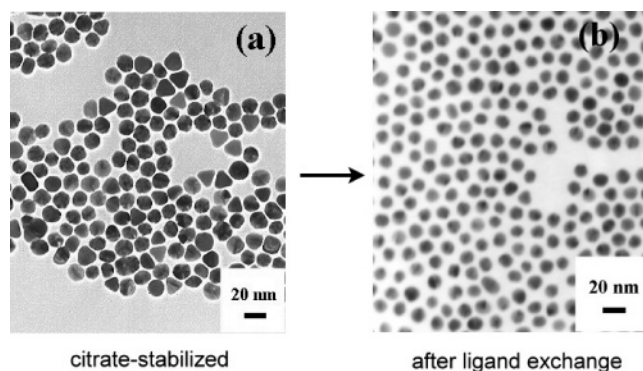


Figure 1. Gold colloids obtained (a) before and (b) after the ligand exchange process. The ligand used here was D2000.

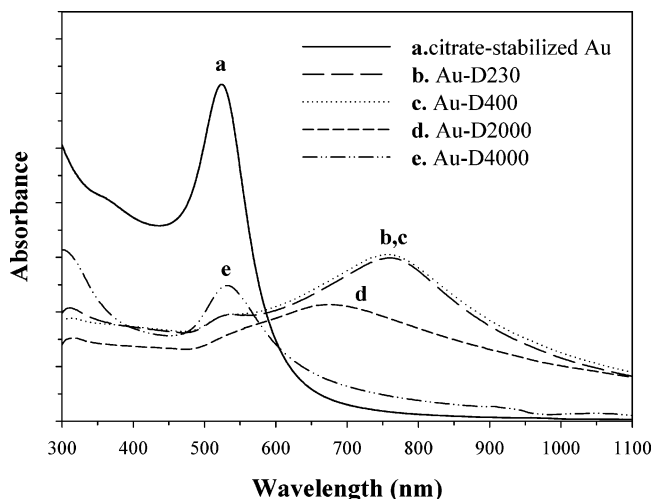


Figure 2. Absorption spectra of the citrate-stabilized gold colloid and those stabilized by different ligands.

We theorize that these changes are the result of an excess of ligand ($[\text{N}]/[\text{Au}^{3+}] = 100$), which now replaces the citrate as the stabilizing agent. The change of electron density on the nanocrystal's surface, together with the change in the adjacent environment caused by the ligand, decreases the attractive interactions between nanocrystals and serves to keep them apart, resulting in the formation of a 2-D monolayer.

While in solution phase, the citrate-stabilized nanocrystals remained well dispersed in the colloid due to electrostatic repulsive interactions in the aqueous trisodium citrate solution and displayed an intense surface plasmon absorption band at 524 nm (Figure 2). After they were mixed with the poly(oxypropylene)diamine ligands, the color of the colloids changed, with the maximum absorption band eventually shifting toward longer wavelengths. Broad absorption bands centered at 759 and 757 nm, respectively, can be seen for the Au-D230 and Au-D400 colloids accompanying a 524 nm shoulder (Figure 2, curves b and c). For Au-D2000 (curve d), we saw a broad peak at approximately 674 nm accompanying the 524 nm shoulder. Au-D4000 (curve e) reveals only a broad peak at 536 nm, which can be deconvoluted into two bands at 529 and 569 nm. It is known that the optical properties of gold colloids are highly dependent on the level of particle aggregation, interparticle separation, and particle size.^{24,25} The broad peaks observed for Au-D230, Au-D400, and Au-D2000 illustrate the fact that the particles are forming aggregates in the solution phase. When gold nanoparticles assemble into 3D structures, there is an increase in the dielectric constant of the medium, shifting the plasmon peak to a lower energy.²⁶ For Au-4000 colloids, the slight shift to 569 nm indicates that the Au particles are forming

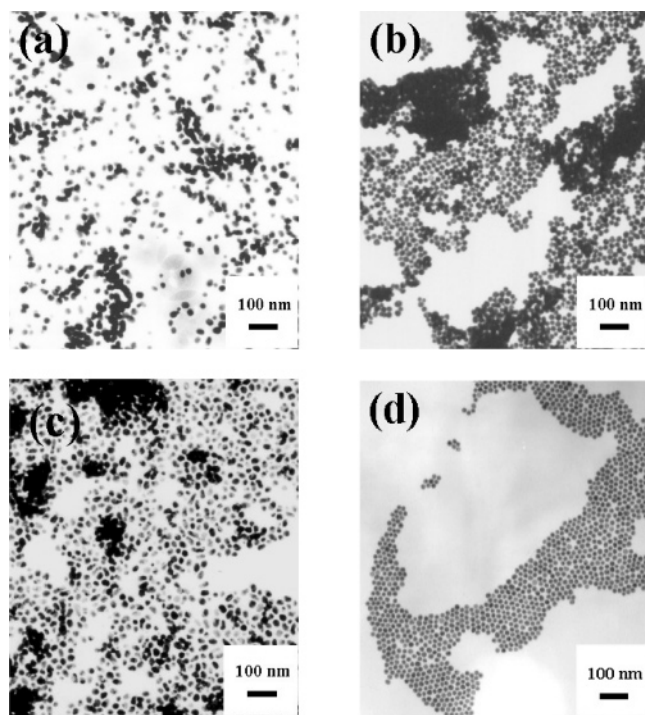


Figure 3. TEM images of Au-D2000 colloids with $[N]/[Au^{3+}]$ ratios of (a) 2, (b) 20, (c) 50, and (d) 100.

a loosely compact structure in the solution phase. These observations in the spectra will be discussed with the interparticle separation in the later section on chain length effect.

Effect of the Ligand Concentration. Although the addition of the ligands allows the nanocrystals to order into a close-packed structure, it is the sizes of the nanocrystals that determine the type of packing that results.²⁷ To evaluate the morphological effect of the ligand concentration, a set of Au colloids was prepared by using D2000 with altered molar ratios of $[N]/[Au^{3+}]$ from 100 to 2. The resulting TEM micrographs of these colloids are shown in Figure 3a–d. For the sample with a very low ligand content, i.e., $[N]/[Au^{3+}] = 2$, as shown in Figure 3a, no assembly is observed. Randomly distributed particles and aggregates are formed with a fairly wide size distribution ranging from 5 to 30 nm. When we increased the ligand concentration, the morphology changed from isolated domains to compact domains, and the particle size gradually became uniform. In regions where a close packing monolayer exists, e.g., in samples with $[N]/[Au^{3+}]$ ratios of 20 and 50, Figure 3, panels b and c, respectively, the resultant assemblies were found to be disrupted by the differences in particle sizes. The addition of a significant excess of amine seems to greatly assist in the formation of ordered assemblies of uniform nanocrystals. This might be due to the fact that more stabilizing dispersion forces have been introduced between the capping molecules.²⁸ Using molecular crystallization as an analogous situation, it is reasonable to propose that better nanocrystalline assemblies with fewer defects are obtained when they are formed slowly.^{29,30} Lin et al. found that adding excess nonvolatile ligands can significantly slow the evaporation rate.²⁷ In our case, it is rational to explain that the addition of excess amines reduces the rate of solvent evaporation, thereby allowing the formation of more regular self-assembled structures.

Structure of Self-Assembly Au Nanoparticles. The formation of metallic Au nanocrystals was confirmed by HR-TEM and selected area electron diffraction (SAED). In a HR-TEM image of Au-D2000 nanocrystals (Figure 4), the particles show lattice images originating from a single crystal. The distances

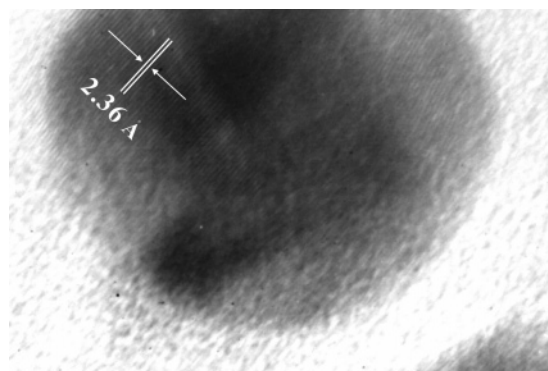


Figure 4. High-resolution image of an individual Au-D2000 nanocrystal.

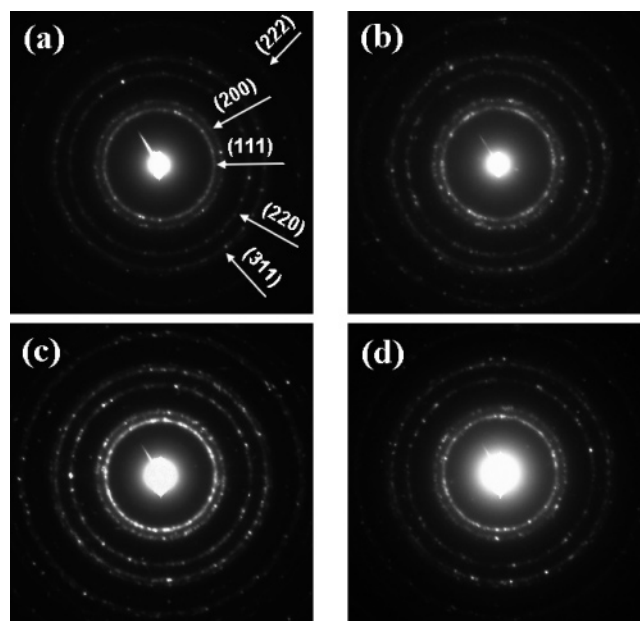


Figure 5. Selected area electron diffraction patterns for (a) Au-D230, (b) Au-D400, (c) Au-D2000, and (d) Au-D4000 nanocrystals.

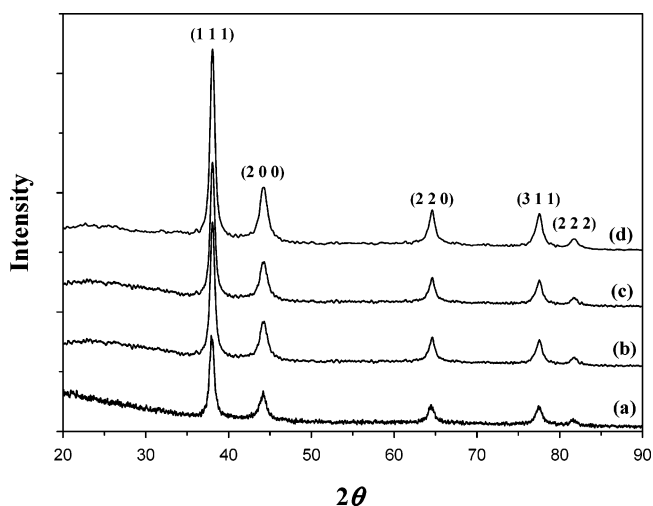


Figure 6. X-ray diffraction patterns of different modified ligands: (a) Au-D230, (b) Au-D400, (c) Au-D2000, and (d) Au-D4000.

between the adjacent lattice fringes, measured as 2.36 Å, are the interplanar distances of the Au $\{111\}$ plane, which are in excellent agreement with the $\{111\}$ d -spacing of bulk Au (2.355 Å). To determine the accurate structures of these nanocrystals, the SAED patterns of more than 200 particles were recorded as shown in Figure 5. The diffraction rings are from

TABLE 1: Size, Particle Gap, Absorption Band, and Potential Energy Analysis of the Gold Nanocrystals before and after the Ligand Exchange

sample	particle size d (nm)		abs band (nm) ^b	particle gap ξ (nm) ^c	E_{vdW} (eV)	ligand thickness l (Å)	chain length (Å) ^d
	TEM	XRD ^a					
citrate stabilized	14.2 ± 1.5		524				
Au-D230	13.9 ± 1.2	13.5	759	2.7 ± 0.7	1.99	29	9
Au-D400	12.0 ± 0.9	12.8	757	2.3 ± 0.8	1.05	27	15
Au-D2000	10.5 ± 0.8	11.7	674	5.3 ± 1.5	0.011	36	77
Au-D4000	17.6 ± 3.4	14.0	529, 569	7.3 ± 1.3	0.018	48	160

^a Particle size calculated from the {1 1 1} peak in XRD measurement. ^b The wavelength of the maximum absorbance band. ^c Mean distance between surfaces of two adjacent particles obtained from TEM images. ^d The theoretical length of the poly(oxypropylene) chain.

the diffraction of the crystal lattice rather than the self-assembled structure. All the detectable dot rings are perfectly indexed to the same positions as those from the face-centered cubic (fcc) structure of standard bulk Au.³¹ The lattice constant (a_0) calculated from the {1 1 1} ring of the Au-D2000 sample (Figure 5c) is 4.087 Å, which is consistent with that of the bulk Au {1 1 1} plane, i.e., 4.079 Å; notably, no differences were obtained with measurements for the other samples.

XRD patterns for the amine-capped gold nanocrystals are shown in Figure 6. Several peaks are observed in every pattern, these being at 38.1°, 44.2°, 64.5°, 77.4°, and 81.6°, which correspond to the {1 1 1}, {2 0 0}, {2 2 0}, {3 1 1}, and {2 2 2} facets³² of the fcc crystal structure, respectively. The interplanar spacing of the {1 1 1} facet, calculated from the diffraction angle of 38.1°, is 2.36 Å, in good agreement with that measured from the above lattice image. The bandwidths become slightly broader for longer POP chain lengths, while the lattice constant remains unchanged. The particle sizes (d) were obtained by measuring the broadening of the {1 1 1} peaks and applying the Scherrer equation^{33,34}

$$d \text{ (nm)} = \frac{k\lambda}{\beta \cos \theta}$$

where k is a constant (0.0368 nm), λ denotes the wavelength of the X-ray used (0.154 nm), β is the full-width half-maximum (fwhm) of the respective diffraction peak (rad), and θ is the angle at the position of peak maximum (rad). The calculated mean diameters of Au-D230, Au-D400, Au-D2000, and Au-D4000 are 13.5, 12.8, 11.7, and 14.0 nm, respectively, these values being close to those obtained by TEM (see Table 1).

Effect of Chain Length. To explore the dependence of Au nanocrystal arrangement on the POP chain length, the solutions capped with D230, D400, D2000, and D4000 ($[N]/[Au^{3+}] = 100$) were immediately deposited on a flat carbon-coated copper grid, and TEM images of the resultant nanocrystals were collected as soon as possible after the solvent evaporated (see Figure 7). These images reveal that the colloids capped with D230 show the formation of mainly densely packed 3-D structures (Figure 7a), with some minor 2-D layers being apparent, indicating that the formation of supracrystal domains occurs quickly in solution. These results coincide with those obtained by absorption spectroscopy. The morphologies of the Au-D400 and Au-D230 colloids look very similar (Figure 7b,a). The Au-D2000 colloids form exclusively 2D ordered monolayers as shown in Figure 7c. For Au-D4000, disordered 3D and 2D structures are present as shown in Figure 7d. Among all the amine-stabilized nanocrystals, Au-D2000 colloids show the greatest monodispersity and readiness to self-assemble into 2D arrays, while the Au-D230 colloids most easily “self-arrange” into 3D structures. Ligand exchange by these amines generally leads to the formation of smaller particles as shown

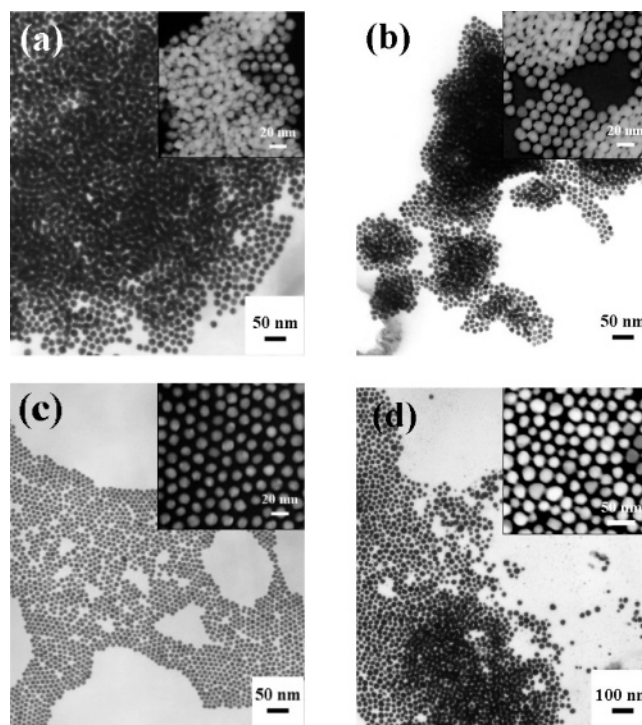


Figure 7. TEM images of the gold nanocrystals modified with different ligands: (a) Au-D230, (b) Au-D400, (c) Au-D2000, and (d) Au-D4000.

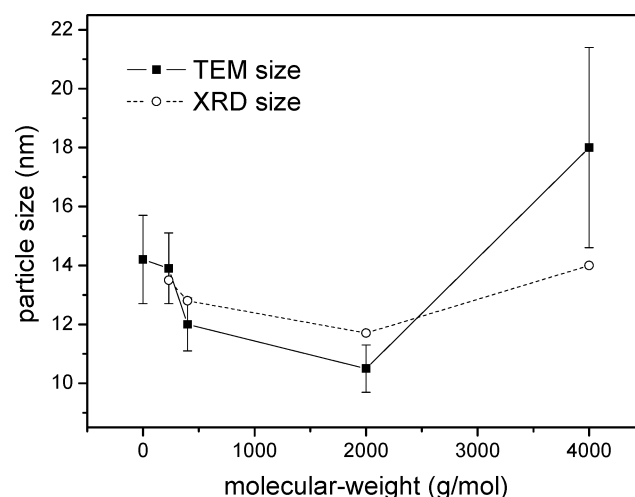


Figure 8. Average particle size as a function of ligand molecular weight. Errors bars are based on the standard deviations.

in Table 1. The dependence of the average particle size, determined from TEM and XRD measurements, on the ligand's molecular weight is shown in Figure 8. Data for citrate-stabilized Au colloids are included at a molecular weight of zero. The relationship between particle size and ligand molecular weight

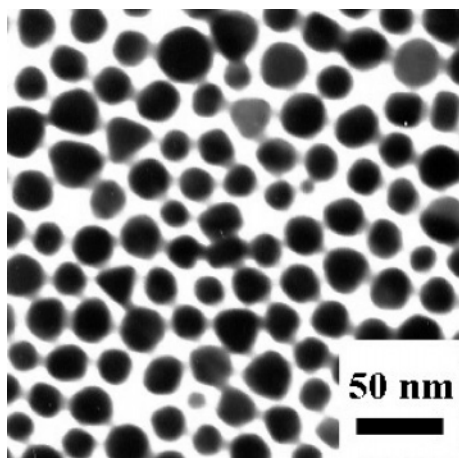


Figure 9. Highlighted image of the same D4000-capped Au colloids seen in Figure 7d showing the existence of ligands (the gray region) between two adjacent particles.

obtained from TEM is similar to that from XRD. For either plot, the dependence of the particle size is nonmonotonic, reaching a minimum for the Au-D2000 sample. In fact, Martin et al.^{15,35} have reported that the dependence of particle size on the thiol alkyl chain length is nonmonotonic with a maximum size being found for decanethiol. Since the molecular structure and theoretical length of the POP chains are definitely different from those of the alkanethiols, a rational explanation for this minima in size found with Au-D2000 is that there is an optimal size for the nanocrystals that allows a most stable packing³⁶ arrangement for the capped POP chains. This explanation will be verified by the stabilization energies calculated from the soft sphere model in a later section.

It is also interesting to note the coherence in the packing order as observed for Au-D4000 colloids (see the highlighted images of the amine-capped particles in Figure 9). It is clear from the literature that the amines may not be firmly attached to the gold surface, thereby allowing more rapid exchange.³⁷ As previously noted, the orientation of the POP chains is not well-defined due to the existence of flexible ether linkages and pendant methyl groups; therefore, there is less of a tendency for the POP chains to form highly ordered close-packed monolayers. This situation could lead to the formation of multilayers of these ligands on a gold crystal surface, with some ligands not being directly attached to the particle's surface. Evidence for this is shown by the particle gaps (ξ) of these nanoparticles (Table 1). D230-capped gold nanocrystals (chain length ~ 8 Å) are separated from each other by about 2.7 nm, and for D400-capped nanocrystals, which have a chain length of about 15 Å, the separation is 2.3 nm, suggesting an interdigitation of POP chains on adjacent amine-ligated particles. The theoretical chain lengths of D2000 (77 Å) and D4000 (160 Å) are much longer than the observed particle gaps of 5 and 7.3 nm, respectively, suggesting a more twisted or folded structure on the particle surface.

In Figure 10a, the particle gaps and the wavelength of the maximum absorbance bands are plotted against the molecular weight of the poly(oxypropylene)diamines. By fitting these data, we find that the absorption bands of ligand-modified Au colloids shift linearly toward the high-energy region with increasing poly(oxypropylene)diamine molecular weights. The particle gap is also found to increase as a function of increasing molecular weight, indicating that the interparticle separation is not proportional to the chain length. The POP chains thus either distort somewhat upon solvent evaporation or tend to interdigitate in the confined space. In Figure 10b, the exponential

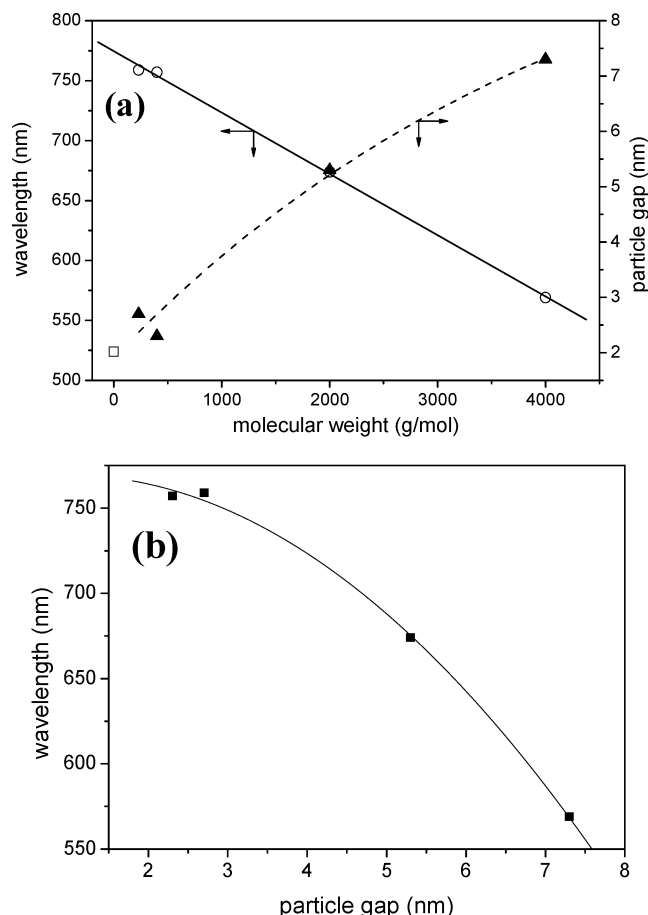


Figure 10. (a) Absorption band (○) and particle gap (▲) of Au colloids change as a function of ligand molecular weight. The absorption band of citrate-stabilized Au nanocrystals (□) is also shown. (b) Gap dependence of the optical absorption of ligand-capped Au nanocrystals.

decrease in the absorption band wavelength with increasing particle gaps is shown. It is well documented now that the optical properties of Au colloids are highly dependent on the level of particle separation. This band in the low-energy region was theoretically predicted by Quinten,³⁸ on the basis that retardation effects and electromagnetic dipolar interactions between different particles would give rise to an additional absorbance at these wavelengths.

According to the report by Thomas et al.³⁹ the experimental observations relating the stability of the Au assemblies to the interparticle distance and particle size find support from empirical calculations based on a soft sphere model.⁴⁰ In this model, the total potential energy (E_t) is considered to be a result of two types of forces between nanocrystals, namely, steric forces and van der Waals forces, eq 1.

$$E_t = E_{\text{steric}} + E_{\text{vdW}} \quad (1)$$

The van der Waals interaction due to polarization of the metal cores constitutes the attractive term, eq 2, and the steric interaction between the ligand molecules on the two surfaces forms the repulsive term,⁴¹ eq 3:

$$E_{\text{vdW}} = \frac{A}{12} \left[\frac{d^2}{\tau^2 - d^2} + \frac{d^2}{\tau^2} + 2 \ln \left(\frac{\tau^2 - d^2}{\tau^2} \right) \right] \quad (2)$$

$$E_{\text{steric}} = \frac{50dl^2}{(\tau - d)\pi\sigma_a} k_B T e^{[-\pi(\tau-d)/l]} \quad (3)$$

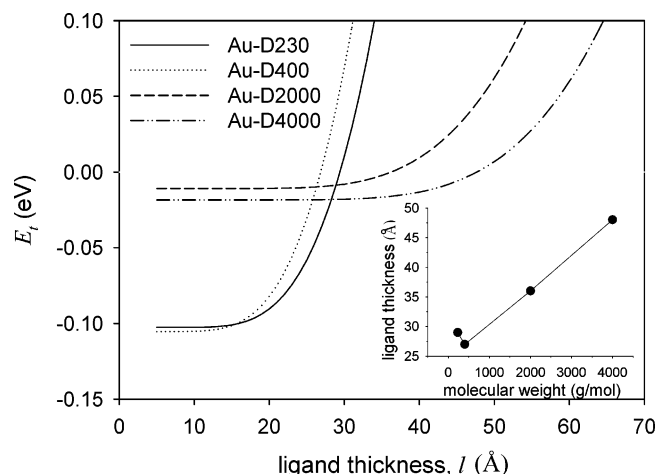


Figure 11. Variation of the total potential energy (E_t) versus ligand thickness (l) for various ligand-capped Au nanocrystals. The plot in the inset shows the dependence of ligand thickness obtained at zero crossover of E_t on the ligand molecular weight.

where τ is the center-to-center distance (interparticle distance) between spheres and A denotes the Hamaker constant⁴² (1.95 eV⁴³ for Au nanoparticles). The calculated diameter of the area occupied by the ligand molecule (σ_a) on the particle surface is 4.3 Å. The van der Waals attraction potentials (E_{vdW}) were found to be 1.99, 1.05, 0.011, and 0.018 eV for Au-D230, Au-D400, Au-D2000, and Au-D4000, respectively. From these data, we can clearly expect Au-D230 and Au-D400 to favor aggregation, since the attraction energies are much higher than the room-temperature thermal energy ($1k_B T = 0.026$ eV), thus enabling them to overcome the solvation energies and room-temperature thermal vibrations more easily than Au-D2000 and Au-D4000. The total energy is attractive over a range of interparticle distances where the attractive energy from the van der Waals term exceeds the repulsive energy due to the steric factor, thereby giving rise to net stabilization of the two-particle system.

Here we have assumed that the two spheres are separated by the POP chain of ligands attached to the Au nanocrystals supposing that the observed particle gaps are at the zero crossover of the total potential energy ($E_t = 0$ eV) against the interparticle distance ($\tau = \xi + d$). This relationship derived from eq 3 is illustrated in Figure 11. The theoretical thickness (l) of the ligand adsorbed on the Au surface can be calculated to be 29, 27, 36, and 48 Å for the Au-D230, Au-D400, Au-D2000, and Au-D4000 colloids, respectively. Plotting the ligand thickness versus the molecular weight (the inset in Figure 11) gives an increase in the ligand thickness on the Au surface of 0.584 Å per 100 g/mol of ligand molecular weight in the range from 400 to 4000 g/mol. We now can determine the stabilization energies of these samples by fitting the above obtained value for l into eq 3 and combining with eqs 1 and 2. As depicted in Figure 12, stabilization energies of 29.4, 25.9, 3.1, and 5.5 meV are obtained from the calculation for nanocrystals capped with D230, D400, D2000, and D4000, respectively. The previous explanation about the minimum in particle size found with Au-D2000 colloids is thus proven by the lowest stabilization energies of 3.1 meV. With shorter POP chain lengths, steep potential energy wells were obtained, strongly suggesting the agglomeration of particles. This result answers well to the band shifts observed in absorption spectra. For longer chain lengths, a shallow minimum exists corresponding to a situation where a thicker ligand layer shields the attractive interactions between the metal cores. An organization of this kind is influenced to a greater extent by the directional property of the POP chains, resulting in less-well-ordered structures.

With the above qualitative results, it is reasonable to assume that the assembly and particle gap of the ligand-capped Au nanocrystals is controlled mainly by the stabilization energy conferred by the packing of ligand molecules on the surface of the Au nanocrystals. The D230 molecules, despite having only a chain length of 8 Å, probably form an end-to-end multilayer

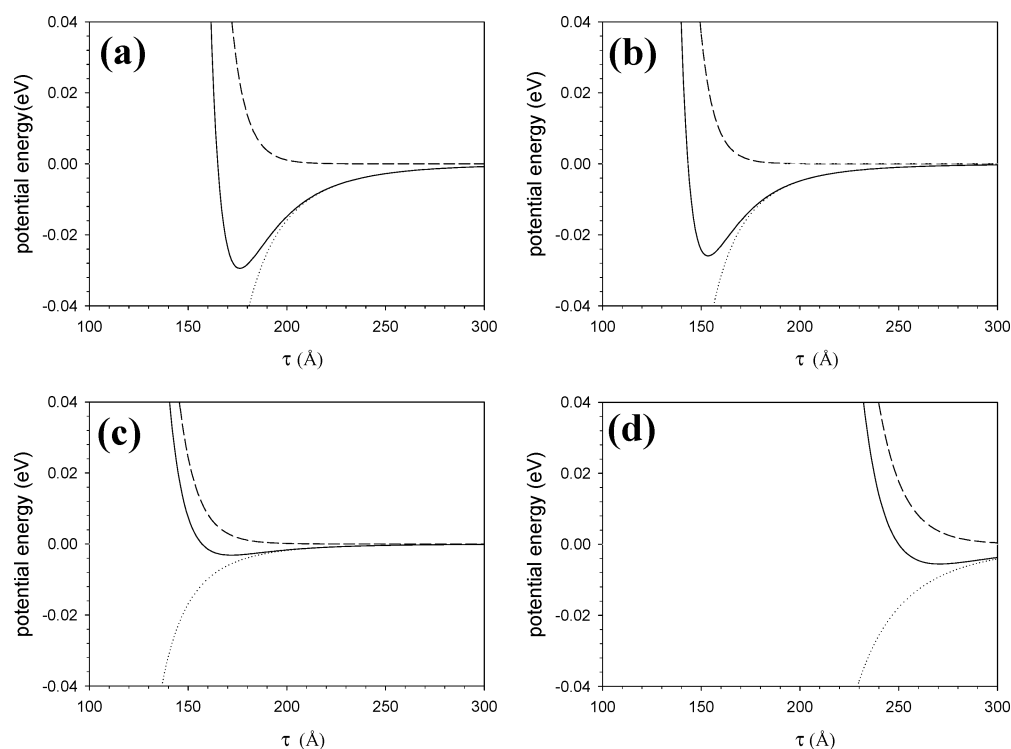


Figure 12. Potential energies (E_t : solid line; E_{vdW} : dotted line; E_{steric} : dashed line) versus the interparticle distance, τ , between two nanocrystals capped with (a) D230, (b) D400, (c) D2000, and (d) D4000.

with a calculated thickness of 29 Å, whereas the D400 molecules (chain length of 15 Å) form an interdigitated bilayer with 27 Å calculated thickness. Both of them are compressed into a fully interdigitated structure with another multilayer on the neighboring particle to form the observed particle gaps of 27 and 23 Å for D230 and D400, respectively. This thin layer is not sufficient to shield the attraction energy between the particles, which results in a more ordered arrangement. For long D2000 molecules, we believe that the 36 Å layer's thickness results from the arrangement of half-bent molecules with an original 77 Å straight chain length, which are also interdigitated with another layer to form bilayer orientation with 50 Å. More twisted molecules of D4000 are expected to form a 48 Å loose layer; this state actually increases the thickness of the ligand layer, and thus minimizes the total potential energy of the system.

Conclusion

We have shown that it is possible to control the particle gap of self-assembled gold nanocrystals over a limited range by capping with poly(oxypropylene)diamine. From TEM images of the ligand-capped gold colloids, we conclude that the minimum particle size and potential energy associated with interparticle attractions results from the most stable packing arrangements for the capped POP chains of a given length. The tendency to form ordered arrays with shorter POP chains and to separate particles with longer chain lengths is rationalized from the decrease in van der Waals attraction potentials as the POP chain length is increased. In addition, we found that the ligand thickness increased by 0.584 Å per 100 g/mol of ligand, for molecular weights in the range of 400–4000 g/mol, and deviates from the theoretical chain length, indicating that D230 may form an end-to-end multilayer. D400 is interdigitated to form a bilayer, while nearly half-bent molecules and randomly twisted molecules probably account for the bilayer of D2000 and the loose structure of D4000, respectively. It is expected that this fundamental framework for self-assembly of ligand-capped nanocrystals will aid the understanding of more sophisticated molecular self-organization scenarios, such as those cases involving different types of ligand chains or different chain lengths.

Acknowledgment. We gratefully acknowledge the National Science Council, Taipei, Taiwan, for their generous financial support of this research.

References and Notes

- (1) Andres, R. P.; Bielefeld, J. D.; Henderson, J. I.; Janes, D. B.; Kolagunta, V. R.; Kubiak, C. P.; Mahoney, W. J.; Osifchin, R. G. *Science* **1995**, *273*, 1690.
- (2) Harfenist, S. A.; Wang, Z. L.; Alvarez, M. M.; Vezmar, I.; Whetten, R. L. *J. Phys. Chem.* **1996**, *100*, 13904.
- (3) Moleller, M.; Spatz, J. P.; Roescher, A. *Adv. Mater.* **1996**, *8*, 337.
- (4) Porter, M. D.; Bright, T. B.; Allara, D. L.; Chidsey, C. E. D. *J. Am. Chem. Soc.* **1987**, *109*, 3559.
- (5) Brust, M.; Walker, M.; Bethell, D.; Schiffrin, D. J.; Whyman, R. *J. Chem. Soc., Chem. Commun.* **1994**, 801.
- (6) Martin, J. E.; Wilcoxon, J. P.; Odinek, J.; Anderson, R. A.; Provencio, P. *J. Phys. Chem. B* **2003**, *107*, 430.
- (7) Lin, X. M.; Sorensen, C. M.; Klabunde, K. J. *Chem. Mater.* **1999**, *11*, 198.
- (8) Kim, B.; Tripp, S. L.; Wei, A. *J. Am. Chem. Soc.* **2001**, *123*, 7955.
- (9) Leff, D. V.; Brandt, L.; Heath, J. R. *Langmuir* **1996**, *12*, 4723.
- (10) Brown, L. O.; Hutchison, J. E. *J. Phys. Chem. B* **2001**, *105*, 8911.
- (11) Nikoobakht, B.; Wang, Z. L.; El-Sayed, M. A. *J. Phys. Chem. B* **2000**, *104*, 8635.
- (12) Yamamoto, M.; Nakamoto, M. *J. Mater. Chem.* **2003**, *13*, 2064.
- (13) Nikoobakht, B.; El-Sayed, M. A. *Langmuir* **2001**, *17*, 6368.
- (14) Prasad, B. L. V.; Stoeva, S. I.; Sorensen, C. M.; Klabunde, K. J. *Chem. Mater.* **2003**, *15*, 935.
- (15) Martin, J. E.; Wilcoxon, J. P.; Odinek, J.; Provencio, P. *J. Phys. Chem. B* **2000**, *104*, 9475.
- (16) Kuo, P. L.; Liang, W. J.; Wang, F. Y. *J. Polym. Sci. Part A: Chem. Ed.* **2003**, *41*, 1360.
- (17) Manna, A.; Imae, T.; Aoi, K.; Okada, M.; Yogo, T. *Chem. Mater.* **2001**, *13*, 1674.
- (18) Kuo, P. L.; Chen, W. F. *J. Phys. Chem. B* **2003**, *107*, 11267.
- (19) Manna, A.; Imae, T.; Iida, M.; Hisamatsu, N. *Langmuir* **2001**, *17*, 6000.
- (20) Kuo, P. L.; Chen, C. C.; Jao, M. W. *J. Phys. Chem. B* **2005**, *109*, 9445.
- (21) Wang, Z. L. *Adv. Mater.* **1998**, *10*, 13.
- (22) Turkevich, J.; Stevenson, P. C.; Hillier, J. *Discuss. Faraday Soc.* **1951**, *11*, 55.
- (23) Mayya, S. K.; Caruso, F. *Langmuir* **2003**, *19*, 6987.
- (24) Storhoff, J. J.; Lazarides, A. A.; Mucic, R. C.; Mirkin, C. A.; Letsinger, R. L.; Schatz, G. C. *J. Am. Chem. Soc.* **2000**, *122*, 4640.
- (25) Mayya, S. K.; Sastry, M. *Langmuir* **1999**, *15*, 1902.
- (26) Galletto, P.; Brevet, P. F.; Girault, H. H.; Antoine, R.; Broyer, M. *J. Phys. Chem. B* **1999**, *103*, 8706.
- (27) Lin, X. M.; Jaeger, H. M.; Sorensen, C. M.; Klabunde, K. J. *J. Phys. Chem. B* **2001**, *105*, 3353.
- (28) Roucoux, A.; Schulz, J.; Patin, H. *Chem. Rev.* **2002**, *102*, 3757.
- (29) Viau, G.; Brayner, R.; Poul, L.; Chakroun, N.; Lacaze, E.; Fiévet-Vincen, F.; Fiévet, F. *Chem. Mater.* **2003**, *15*, 486.
- (30) Bönnemann, H.; Richards, R. M. *Eur. J. Inorg. Chem.* **2001**, 2455.
- (31) Teranishi, T.; Hosoe, M.; Tanaka, T.; Miyake, M. *J. Phys. Chem. B* **1999**, *103*, 3818.
- (32) Shimizu, T.; Teranishi, T.; Hasegawa, S.; Miyake, M. *J. Phys. Chem. B* **2003**, *107*, 2719.
- (33) Li, X.; Li, Y.; Tan, Y.; Yang, C.; Li, Y. *J. Phys. Chem. B* **2004**, *108*, 5192.
- (34) Cullity, B. D. *Element of X-ray Diffraction*, 2nd ed.; Addison-Wesley: Menlo Park, CA, 1978.
- (35) Prasad, B. L. V.; Stoeva, S. I.; Sorensen, C. M.; Klabunde, K. J. *Langmuir* **2002**, *18*, 7515.
- (36) Sawyer, L. C.; Grubb, D. T. *Polymer Microscopy*, 2nd ed.; Chapman & Hall: New York, 1996.
- (37) Ulman, A. *Chem. Rev.* **1996**, *96*, 1533.
- (38) Quinten, M.; Kreibitz, U. *Surf. Sci.* **1986**, *172*, 557.
- (39) Thomas, P. J.; Kulkarni, G. U.; Rao, C. N. R. *J. Phys. Chem. B* **2000**, *104*, 8138.
- (40) Korgel, B. A.; Fullam, S.; Connolly, S.; Fitzmaurice, D. *J. Phys. Chem. B* **1998**, *102*, 8379.
- (41) Ohara, P. C.; Leff, D. V.; Heath, J. R.; Gelbart, W. M. *Phys. Rev. Lett.* **1995**, *75*, 3466.
- (42) Hamaker, H. C. *Physica (Utrecht)* **1937**, *4*, 1058.
- (43) Korgel, B. A.; Fitzmaurice, D. *Phys. Rev. Lett.* **1998**, *80*, 3531.